




Predicting regime changes and durations in Lorenz's atmospheric convection model

Cite as: Chaos **30**, 103109 (2020); <https://doi.org/10.1063/5.0013253>

Submitted: 09 May 2020 . Accepted: 24 September 2020 . Published Online: 08 October 2020

Eduardo L. Brugnago , Jason A. C. Gallas , and Marcus W. Beims 



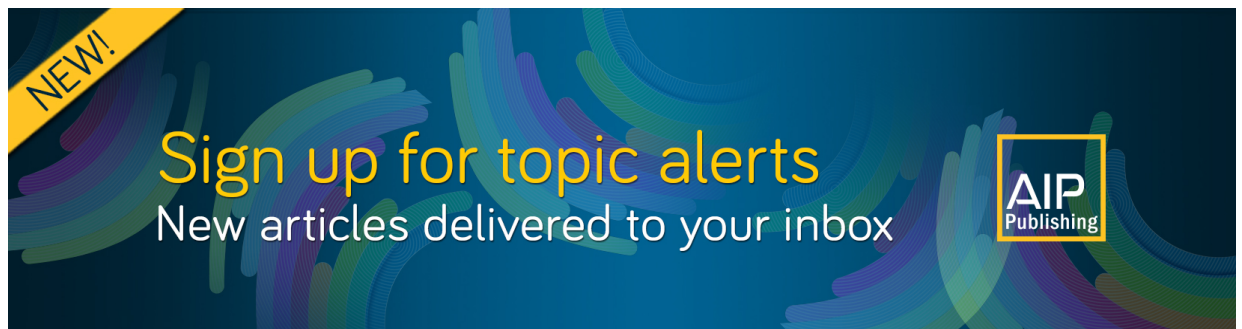
View Online



Export Citation



CrossMark



NEW!

Sign up for topic alerts

New articles delivered to your inbox

AIP Publishing



Predicting regime changes and durations in Lorenz's atmospheric convection model

Cite as: Chaos 30, 103109 (2020); doi: 10.1063/5.0013253

Submitted: 9 May 2020 · Accepted: 24 September 2020 ·

Published Online: 8 October 2020



View Online



Export Citation



CrossMark

Eduardo L. Brugnago,^{1,a)} Jason A. C. Gallas,^{2,3,4,b)} and Marcus W. Beims^{1,2,c)}

AFFILIATIONS

¹Departamento de Física, Universidade Federal do Paraná, 81531-980 Curitiba, Brazil

²Max Planck Institute for the Physics of Complex Systems, Nöthnitzer Str. 38, 01187 Dresden, Germany

³Instituto de Altos Estudos da Paraíba, Rua Silvino Lopes 419-2502, 58039-190 João Pessoa, Brazil

⁴Complexity Sciences Center, 9225 Collins Avenue Suite 1208, Surfside, Florida 33154, USA

^{a)}elb@fisica.ufpr.br

^{b)}jason.gallas@gmail.com

^{c)}Author to whom correspondence should be addressed: mbeims@fisica.ufpr.br

ABSTRACT

We show that a characteristic alignment between Lyapunov vectors can be used to predict regime changes as well as regime duration in the classical Lorenz model of atmospheric convection. By combining Lyapunov vector alignment with maxima in the local expansion of bred vectors, we obtain an effective and competitive method to significantly decrease errors in the prediction of regime durations.

Published under license by AIP Publishing. <https://doi.org/10.1063/5.0013253>

Forecasting the dynamics in complex systems is nowadays one of the outstanding challenges for researchers around the world. So far, there is no adequate physical quantity capable of making precise predictions about the future in chaotic systems. Therefore, any additional method or property that helps the predictability mission is most welcome. Recently, it was shown that the alignment between Lyapunov vectors is closely related to the occurrence of extreme and rare events in chaotic systems and that such alignments can help to predict rare events. This key piece of information is used here to predict regime changes as well as regime duration in the paradigmatic Lorenz 1963 model of atmospheric convection. We show how to combine two familiar tools, namely, Lyapunov vector alignment with maxima observed in the local expansion of bred vectors, to significantly decrease errors in the prediction of regime durations, thereby providing competitive predictions for the onset of large and possibly catastrophic events. These combined tools seem to be particularly well suited for complex systems displaying two-wing (Lorenz's case) or multiple-wing chaotic attractors.

I. INTRODUCTION

The ability to predict the future based on past and present data is of high relevance in several distinct areas such as, e.g.,

forecasting climate changes, stock markets, virus propagations, critical transitions, extreme and rare events, which include giant ocean waves, extreme weathers, lasers peaks, among others.¹ The dynamics in such realistic problems is typical of highly nontrivial high-dimensional complex systems, and there is no model that can fully describe them. Instead of using models, several forecasting methods rely directly on data sources from the real world itself. Therefore, forecasting dynamical behaviors of complex systems is an extremely challenging open problem. Using distinct methods, considerable effort to improve forecasting tools has been done during the last few years, including machine learning techniques.² The main issue, however, namely, to reveal the fundamental principles behind the mechanism of predicting the future remains obscure. In this context, a significant development^{3,4} toward understanding the mechanism behind forecasting was the observation that an *alignment* of Lyapunov vectors (LVs) occurs *before* the appearance of large peaks in chaotic three-dimensional continuous systems.

The goal of this work is to show that the alignment of LVs is able to predict not only regime changes, but also the *duration* of individual regimes as described by the standard Lorenz model of atmospheric convection.⁵ Before a change of a given regime, the LV of the most unstable direction is found to align along the flow direction, characterized by the direction of the LV associated with the zero Lyapunov exponent. The LVs considered here are

the covariant Lyapunov vectors.⁶ They are obtained by integrating the equations of motion forward and backward along the same trajectory^{6–11} and have been calculated in a multitude of realistic systems, such as systems coupled to deterministic thermal reservoir,¹² in cluster synchronization of scale-free networks of chaotic maps,¹³ the regeneration cycle in wall turbulence,¹⁴ in the traffic of vehicles,¹⁵ to describe dynamical trapping in conservative maps¹⁶ and the transformation of conservative tori in dissipative sinks,¹⁷ interacting neutrino gas,¹⁸ turbulence in a partial differential equation,¹⁹ a toy model in ocean-atmosphere,⁹ angle enhanced bifurcation diagrams in the Hénon map,²⁰ hyperbolicity estimation in 2D chaotic maps,²¹ super-Lyapunov growth in the Lorenz system,²² periodic windows corresponding to unstable periodic orbits,²³ to predict critical transitions,²⁴ among others. In all these systems, the LVs were used in different ways for a deeper understanding of the dynamics. As it is well-known,²⁵ for certain parameter values, the Lorenz model displays a characteristic butterfly-looking two-wing chaotic attractor, illustrated in Fig. 1, arising from back-and-forth oscillations around two unstable fixed points of the system. It is common to associate oscillations around each such wing of the butterfly to a weather regime, designating them *right* (*R*) and *left* (*L*) regimes. The possibility to predict regime changes, and their duration, has been studied earlier using the concept of bred vectors (BVs)²⁶ and the maximum of a peak (for a given variable) right before the regime changes.²⁷

In the present work, we show that the alignment of LVs is more efficient to predict regime changes when compared to predictions made solely by bred vectors and somewhat similar to a methodology that uses the aforementioned maxima of the peaks of one variable. The alignment of LVs gives a clear mathematical description of the ability to predict regime changes and regime durations. We found a direct relation between the alignment of LVs and the predicted regime duration. In other words, once the alignment of LVs is observed, it is possible to estimate the duration of the predicted regime. By suitably combining results obtained for LVs and BVs, we significantly decrease the amount of errors in the regime prediction times.

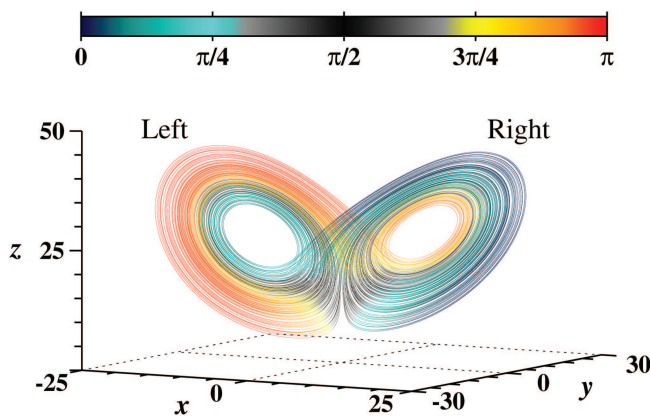


FIG. 1. Angle enhanced Lorenz attractor in (x, y, z) coordinates and colors indicate the values of the angle θ between the unstable invariant manifold and the flow direction.

The paper is organized as follows. In Sec. II, we present briefly the Lorenz model and display the angle enhanced chaotic attractor for specific parameters of the model. Sections III and IV describe, respectively, the ability of the alignment of LVs to predict regime changes and regime lengths. In Sec. V, we illustrate a new way to use properties of the bred vectors to predict regime times. Section VI describes how to improve errors in the prediction times by combining results for LVs and BVs. Section VII summarizes our main results.

II. THE LORENZ SYSTEM AND THE ANGLE ENHANCED ATTRACTOR

The 1963 Lorenz model of atmospheric convection is governed by the flow,⁵

$$\dot{x} = \sigma(y - x), \quad (1)$$

$$\dot{y} = rx - y - xz, \quad (2)$$

$$\dot{z} = xy - bz, \quad (3)$$

where (x, y, z) are dimensionless variables that evolve in continuous time t , $(\dot{x}, \dot{y}, \dot{z})$ are the associated velocities, and (σ, r, b) are real and positive parameters.

In Fig. 1, a typical trajectory is shown for $\sigma = 10$, $b = 8/3$, and $r = 28$, starting from the initial condition close to the unstable fixed point at $x = 0.1$, $y = 0.2$, and $z = 30$. For these parameters, the attractor in Fig. 1 has Lyapunov exponents $\lambda_1 = 0.91$, $\lambda_2 = 0.00$, and $\lambda_3 = -14.6$, calculated in the natural logarithm base. One Lyapunov exponent is always zero since the dynamics is a flow, i.e., time continuous. The associated unitary covariant LVs are \mathbf{v}_1 , \mathbf{v}_2 , and \mathbf{v}_3 , pointing along the unstable, flow and stable invariant manifold directions, respectively. The angles between the LVs are then determined for each integration time from the expression $\varphi_{ij} = \cos^{-1}(\mathbf{v}_i \cdot \mathbf{v}_j)$. In this work, we used only the angle $\theta = \varphi_{12}$, i.e., the angle between the unstable manifold and the flow direction.

In Fig. 1, colors represent the values of the angle θ along the trajectory. Equations (1)–(3) were solved numerically using a standard fourth-order Runge–Kutta algorithm with a fixed time step $h = 0.05$. The first 10^7 time steps were discarded as transient, and the LVs were computed subsequently for 6×10^5 time steps (including forward and backward time motion).

As mentioned, the Lorenz attractor is well-known, being essentially the combination of two connected spiraling motions, one on the right, for (x, y) positive, and another one on the left, for (x, y) negative. Each spiral represents a regime denoted as *R* (right one) and *L* (left one). From Fig. 1, we observe that the external portion of the spirals in different regimes has distinct values of θ , namely, $[0, \pi/2]$ for the *R* loops and $[\pi/2, \pi]$ for the *L* loops. In addition, on the top border of each loop, θ tends to become close to 0 for *R* and close to π for *L*. For details about plotting angle enhanced attractors, see Ref. 20.

III. PREDICTING REGIME CHANGES

The time series for the variables (x, y) of the representative trajectory shown in Fig. 1 consists of oscillations inside the regime and some regime changes when oscillations escape to the other butterfly

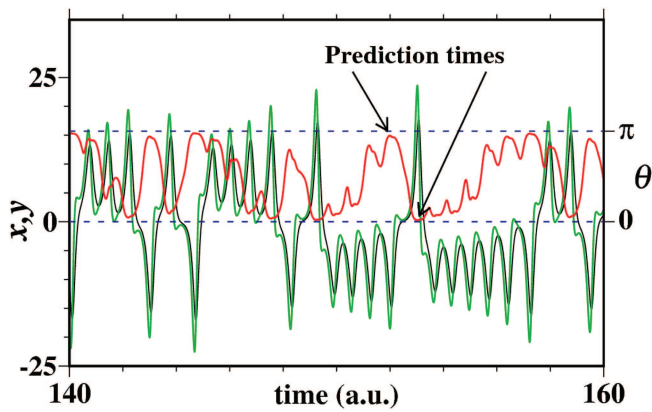


FIG. 2. Time evolution of x (black curve), y (green curve), and θ (red curve). For reference, the pair of dashed horizontal lines (blue) marks the values of 0 and π . Arrows indicate representative prediction times.

wing. This time evolution can be better observed in the time window shown in Fig. 2. For better visualization, in this figure, we plot the system’s variables in a different scale than the angle. The black curve is the variable x , the green curve the variable y , and the red curve the angles θ .

Clearly, one sees that the variables (x, y) change sign, (i.e., change regime) almost simultaneously. Interesting is that *before* regime changes, θ comes close to zero for changes $R \rightarrow L$ and close to π for changes $L \rightarrow R$. Two examples of such prediction times are indicated by the black arrows in Fig. 2. This behavior can be checked visually in Fig. 2 for almost any regime change, suggesting that changes are to be expected for times after which

$$\theta \rightarrow \theta^{(\min)} \approx 0 \quad \text{for } R \rightarrow L$$

or

$$\theta \rightarrow \theta^{(\max)} \approx \pi \quad \text{for } L \rightarrow R.$$

The values $\theta^{(\min)} \approx 0$ and $\theta^{(\max)} \approx \pi$ correspond to the alignment of the unstable manifold along the flow direction, i.e., the alignment of LV \mathbf{v}_1 along the flow direction.

In order to give a quantitative description of regime forecasting, we analyze in more detail the attractor shown in Fig. 1. Altogether, it contains 1728 regime changes, and all of them can be predicted for a given time by looking at the values of θ . The difference between the time for which a regime change occurs and the time for which $\theta \rightarrow \theta^{(\min)}$ [or $\theta \rightarrow \theta^{(\max)}$] is called lead time. The lead time as a function of $\theta^{(\min)}$ and $\theta^{(\max)}$, obtained right before the regime changes, is plotted in Fig. 3. Thus, there is an associate lead time for each angle that approaches $\theta \rightarrow \theta^{(\min)}$ [or $\theta \rightarrow \theta^{(\max)}$].

Our results show that for angles very close to 0 or π , the lead times are shorter, close to 0.2. Larger lead times for regime changes can be obtained for values away from 0 or π . For the integrated times, no regime changes are observed when $\theta^{(\min, \max)}$ is inside the interval $[3\pi/8, 5\pi/8]$. Figure 3 also illustrates the symmetry of lead times between angles $\theta^{(\min, \max)}$. In other words, lead times are symmetric between $R \rightarrow L$ and $L \rightarrow R$. Due to the peaks and valleys

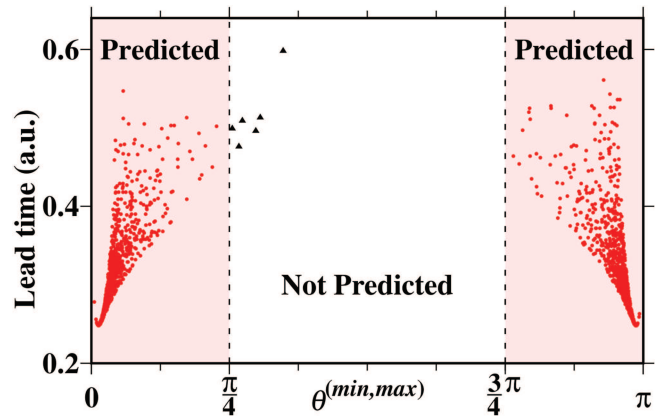


FIG. 3. Lead time plotted as a function of the minimum (between 0 and $\pi/4$) and maximum (between $3\pi/4$ and π) angles. Dark triangles in the middle represent times before regime changes that our method could not predict.

preceding the maximum and minimum within each regime, we only consider values less than $\pi/4$ away from the alignment.

Next, we evaluate the ability of the alignment of LVs to predict regime changes when compared to methods that use bred vectors²⁶ and the maxima of the peaks (MP).²⁷ To obtain bred vectors, consider a reference trajectory \mathcal{A} and a perturbed trajectory \mathcal{P} . The modulus of the BVs ($|\mathbf{B}| = B$) is the Euclidean distance between \mathcal{P} and \mathcal{A} , determined at the end of each breeding cycle. In the case of BVs, two rules were used: 1 BV—when the BV exceeds 0.064 during eight steps of the time evolution, then the regime will change and 2 BV—the duration of the new regime is proportional to the number of eight BV steps that exceeded 0.064 in the previous regime. Table I reproduces results obtained from BVs as reported in Ref. 26. For example, in the first line of Table I, the 1 BV rule was able to predict correctly 187 regime changes and 13 false alarms from a total of 200 regime changes. This gives a hit rate of 93.5%, which is the percentage of the predictions correctly anticipating a subsequent change (or lack) of regime. The false alarm rate is 6.5%, which is the percentage of predicted regime changes that did not occur.

In the case of MP, there are two simpler rules, namely, 1 MP—when $x(t) \gtrsim 14.8$, the current regime will change and 2 MP—the length of the new regime increases monotonically with the maximum value of $|x(t)|$ from the previous regime. Table I also reproduces the results obtained from rule 1 MP as given in Ref. 27.

TABLE I. Number of forecasted/observed regime changes using rules for BV|MP|LV (BV and MP are reproduced from Refs. 26 and 27, respectively).

Fcst/Obs	Yes			No			Total		
	BV	MP	LV	BV	MP	LV	BV	MP	LV
Yes	187	266	1722	13	0	0	200	266	1722
No	33	1	6	299	386	0	332	387	6
Total	220	267	1728	312	386	0	532	653	1728

The hit rate is now 99.65% and not predicted cases are 0.35%, missing to predict only one regime change, as can be observed in the second line of Table I.

In the case of the alignment of LVs, the rules are as follows: 1 LV—when the angles are $0 \leq \theta^{(\min)} \lesssim \pi/4$ and $3\pi/4 \lesssim \theta^{(\max)} < \pi$, the current regime will change and 2 LV—the length of the new regime increases monotonically with $\theta^{(\min)}$ approaching zero and $\theta^{(\max)}$ approaching π (this property will be demonstrated in Sec. IV). Applying rule 1 LV, our results regarding hit rates and false alarms are presented in Table I. The efficiency is similar to the MP procedure. We mention, however, that the alignment of LVs is able to predict any regime change in the Lorenz system by letting rule 1 LV be very flexible.

IV. PREDICTING REGIME DURATION

Remarkable behavior is obtained when correlating the angles $\theta_n^{(\min, \max)}$ with the duration of the regime predicted by them, defined as Δt_{n+1} , where the index n identifies the n th regime. This is illustrated in Fig. 4, where Δt_{n+1} is plotted as a function of the minimal and maximal angles used to predict Δt_{n+1} . In this section, we expand our analysis to 5×10^6 regimes. Figure 4 clearly shows that, as $\theta_n^{(\min)} \rightarrow 0$ and $\theta_n^{(\max)} \rightarrow \pi$, the duration of the regime they predict increases very fast. The discreteness observed in the values of Δt_{n+1} arise because regime changes occur only when the variables (x, y) cross the origin. Consecutive crossings can only occur after one oscillation of these variables (see Fig. 2). This can be checked by comparing the interval of discreteness in Fig. 4, which is around 0.8 (a.u.), this being the average time of one turn in each spiral. We mention that the qualitative behavior in the plane $\Delta t_{n+1} \times \theta_n^{(\min, \max)}$, presented in Fig. 4, is somewhat similar to the behavior presented in Ref. 27 using the MP method. Due to the discreteness, a clustering of points at specific values of Δt_{n+1} is observed.

The number of laps (rotations) around the unstable fixed point for each regime can be used to classify the clusters, as indicated by the numbers in the insets (a) and (b) from Fig. 4. The number of laps during a regime is associated with the duration of the regime and is given, directly, by the number of peaks (right regimes) or valleys (left regimes) in the time series of the x variable.² Thus, each cluster has a fixed value of laps. Regimes with longer durations have a larger number of laps. Such classification considering the number of peaks or valleys inside the regimes was used recently to train multi-layer perceptron.^{2,31} The density of points in Fig. 4, when $\theta_n^{(\min)} \rightarrow 0$ and $\theta_n^{(\max)} \rightarrow \pi$, suggests that regimes with long durations are rare. Numerical results confirm that while regimes with a short duration occur very often, regimes having a long duration tend to be extreme and rare events. In other words, from Fig. 4, we conclude that these extreme and rare events can be predicted only when $\theta_n^{(\min, \max)}$ is very close to 0 or π , respectively.

In order to understand the average behavior of the relationship between the duration Δt_{n+1} of the regimes and the angles $\theta_n^{(\min, \max)}$, we determined the centroid of the clusters (blue stars in Fig. 4) and adjusted a curve for each side (L and R) according to these points. In the same figure, the red curves represent the fitting given by

$$\Delta t_{\text{fit}}^{(\min)} = a_1 + \frac{b_1}{[1 + c_1 \theta_n^{(\min)}]^{d_1}}, \quad R \rightarrow L, \quad (4)$$

$$\Delta t_{\text{fit}}^{(\max)} = a_2 + \frac{b_2}{[1 + c_2 (\pi - \theta_n^{(\max)})]^{d_2}}, \quad L \rightarrow R. \quad (5)$$

Given the symmetry in the distribution of the points in Fig. 4, it is expected that the constants of the same position in Eqs. (4) and (5) are equal. However, small numerical differences lead to different values for these constants, being

$$a_1 = 0.179, \quad b_1 = 15.9, \quad c_1 = 36.1, \quad d_1 = 1.56,$$

$$a_2 = 0.254, \quad b_2 = 15.7, \quad c_2 = 32.7, \quad d_2 = 1.67.$$

In Fig. 4, the inset (a) displays a magnification of a region near the minimum of the angle θ . This plot highlights the numbered clusters formed in the plane $\theta_n^{(\max)} \times \Delta t_{n+1}$, as already mentioned, due to the number of laps within the regime. The red line shows that the cluster average Δt_{n+1} increases very fast when approaching the extreme angles, as proposed in Eq. (5). Projections of overlapping islands on the angle axis are highlighted in inset (b). Such features lead to an error factor for predicting regime durations. For example, the vertical dashed line indicates a value for the angle, $\theta_n^{(\max)} = 3.06$, for which there is an uncertainty between two islands and the prediction curve points to the central value. To solve this, in Sec. VI, we propose a solution for this uncertainty and improve predictions by combining the data from this section with data from bred vectors.

The overlapping of the projection of the clusters on the angle axis, observed in the Fig. 4, leads to prediction errors. When more clusters overlap, more significant is the error. A function that relates the angles to the durations of the regimes will always bring a considerable error. We quantify the MSE (Mean Square Error) resulting from a step function, used as the prediction function, in the same

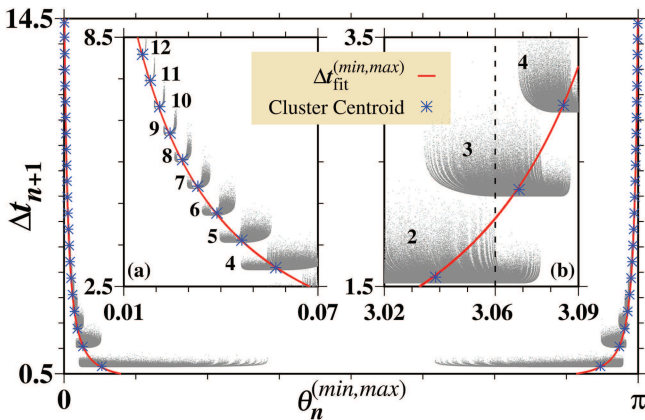


FIG. 4. Regime duration Δt_{n+1} as a function of the minimum and maximum angle $\theta_n^{(\min, \max)}$ in each regime. Red curves represent a fit and blue stars mark the cluster centroid. The inset (a) highlights the classification of clusters and (b) amplifies a region where one value of $\theta_n^{(\max)}$ corresponds to several values of Δt_{n+1} . The numbers shown for each cluster are the number of laps around the unstable fixed point at the lobe center for each regime. See the text.

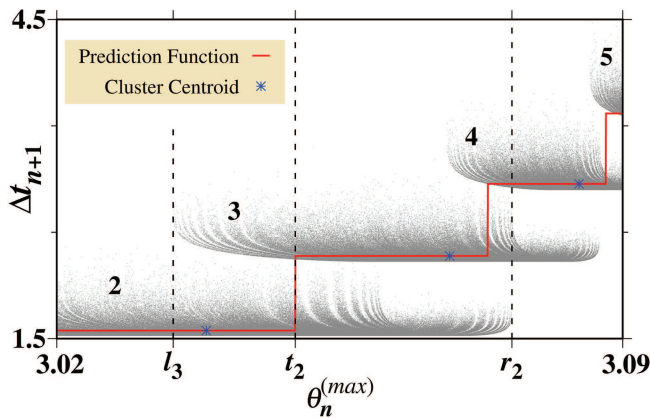


FIG. 5. Regime duration Δt_{n+1} as a function of the minimum and maximum angle $\theta_n^{(\min,\max)}$ in each regime for a specific interval of angles. Red curves are the adjustment from Eq. (6) and blue stars mark the cluster centroid.

range of angles as the inset in Fig. 4(b),

$$D(\theta_n^{(\max)}) = C_i, \text{ being } t_{i-1} \leq \theta_n^{(\max)} < t_i. \quad (6)$$

Here, D is the predicted duration for the next regime, C_i is the value of the ordinate in the centroid of the i th cluster, and t_i the transition between cluster i and $i + 1$. In the range $3.02 \leq \theta_n^{(\max)} \leq 3.09$, we do not need to define t_0 . In Fig. 5, we illustrate the behavior of Eq. (6) (red curve) together with the numbered clusters. It is important to mention that $t_{i+1} < t_i < r_i$, where t_{i+1} is the left extreme of the $(i + 1)$ th cluster and r_i is the right extreme of the i th cluster, as shown by the dashed vertical lines in Fig. 5. The transition point t_i from one cluster to the next one is determined so that in the interval $[t_i, r_i]$, the i th cluster has fewer points than the following.

We calculate the MSE between the predicted curve and the data from

$$MSE = \frac{1}{N} \sum_n \left[D(\theta_n^{(\max)}) - \Delta t_{n+1}^{(\max)} \right]^2, \quad (7)$$

where $3.02 \leq \theta_n^{(\max)} \leq 3.09$ and N is the number of points in this range. For the example shown in Fig. 5, the result is $MSE = 0.320$.

Another way of obtaining a forecast for the duration of the regimes is to assign a value using the average of the nearest neighboring points. We use this technique, called k -NN (k -Nearest Neighbors),^{28,29} to determine the $k = 3$ angles within the dataset closest to a test angle. Once the nearest points are determined, the expected duration is the average of the durations at those points. To determine the error in the forecast, we also calculate the MSE between the predicted values and the data. Although there is a considerable overlap and the determination of the neighborhood outside is only one dimensional, we obtain $MSE = 0.198$, a significant improvement when compared to the previous result. The use of this method is essential for the comparison we make in Sec. VI since we use the same technique there. For the tests, the data were randomly separated into two sets of the same size, the first for the test points and the other for the reference points.

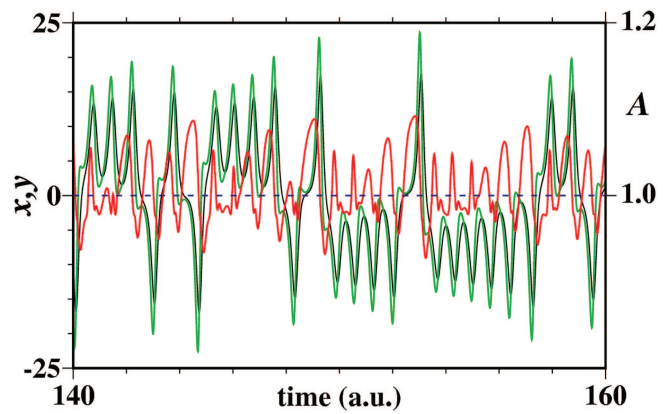


FIG. 6. Variables x (black), y (green), and A (red) in a time window. In this case, a transient of 10^5 was discarded and the integration step is $\delta = 10^{-3}$.

V. THE INCREASE OF BRED VECTORS

To display a more significant variation of the bred vectors, the modulus is calculated after every eight integration steps and then renormalized with a new perturbation in \mathcal{P} . The initial distance between reference and perturbed trajectories is 10^{-2} . We have also checked larger perturbations, but they lead to convergence problems of the bred vectors. Smaller values of the perturbations should tend to Lyapunov results. Thus, the prediction quality should not be affected very much by the initial perturbation. Therefore, the rate of increase of the bred vectors is given by the ratio $A(t) = B(t)/B(t - 8\delta)$: $A(t) < 1$ indicates an approach of the trajectories \mathcal{P} and \mathcal{A} , while $A(t) > 1$ indicates separation. Here, $\delta = 10^{-3}$ is the integration time step.

Figure 6 illustrates behavior of $A(t)$ (red curve) for a time window and compares it to the variable $x(t)$ (green curve). Note that maxima of $A(t)$ in each regime occur in close regime changes. As for LVs, this behavior can be used to predict the regime changes.

There is, however, an essential distinction between using LVs or the maxima of $A(t)$. The angle $\theta_n^{(\min,\max)}$ in Fig. 2 is always above or below a threshold $\pi/2$. For example, for times around 144 (a.u.), a change $R \rightarrow L$ occurs and θ remains smaller than $\pi/2$ in the beginning of regime L . After some time in L , θ becomes larger than $\pi/2$ and remains so until a new regime change is observed. There are no multiple oscillations of θ around $\pi/2$ within one regime. The transition of θ across the threshold $\pi/2$ is already an indication that a regime change will occur. Such an indication cannot be made for $A(t)$ in Fig. 6 since no threshold is observed. In the $A(t)$ method, long regimes are preceded by the most pronounced local extremes in $A(t)$. In order to relate these local maxima with the duration of the forthcoming regimes, we define $A_n^{(\max)} = \max\{A(\tau_n < t < \tau_{n+1})\}$, where τ_n is the time starting the n th regime.

Figure 7 illustrates typical results for Δt_{n+1} as a function of $A_n^{(\max)}$. This figure shows clearly that larger values of $A_n^{(\max)}$ are associated with longer regime durations. Again, a clustering of points is observed, resembling results already seen in Fig. 4.

Similarly to Sec. IV, we identified the cluster centroid (blue stars in Fig. 7) and numbered the clusters according to the turns

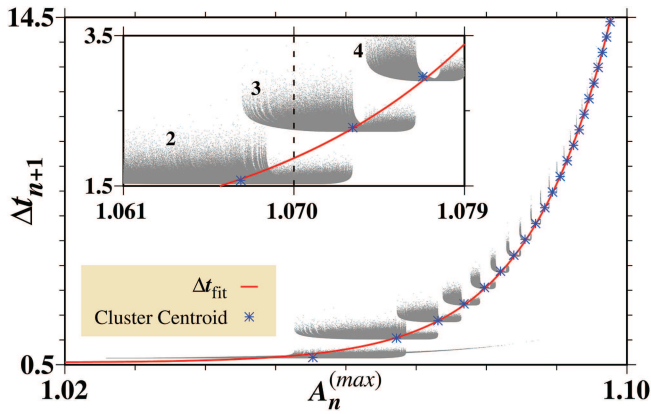


FIG. 7. Pairs $(A_n^{(max)}, \Delta t_{n+1})$ in gray. The fitted curve Δt_{fit} from Eq. (8) is shown in red and the cluster centroid indicated by blue stars.

taken within the regime, as shown in the inset. We derive a curve to fit the centroids, namely,

$$\Delta t_{fit} = f + g [A_n^{(max)}]^h. \quad (8)$$

Here, the parameters used are $f = 0.580$, $g = 0.00234$, and $h = 93.2$, which correspond to the red curve in Fig. 7.

As with the angles, the overlap of the horizontal projection of clusters (see the inset in Fig. 7) leads to prediction errors. Here, we do not include examples of determining these errors.

VI. IMPROVED PREDICTION OF REGIME DURATION

A relevant error in the prediction of the regime duration arises when we observe in Fig. 4 that for specific values of $\theta_n^{(min,max)}$ in regions with high overlapping, as shown in the inset of Fig. 4(b), more than one value of $\Delta t_{n+1}^{(min,max)}$ is possible. Besides, inside each cluster, the values of $\Delta t_{n+1}^{(min,max)}$ vary. This occurs because the clustering of points emerges superposed for certain values of either $\theta_n^{(min)}$ or $\theta_n^{(max)}$. The same difficulty may be recognized in Fig. 7 since for one value of $A_n^{(max)}$, more values of Δt_{n+1} are possible. Even if we use Eqs. (4), (5), and (8), some error in the determination of the correct predicted regime duration will occur due to the discretized aspect of the succession of clusters.

One way to decrease the amount of errors due to cluster superposition is to increase the dimension of the available quantities for the prediction. To do so, we combine results from Figs. 4 and 7. In other words, we combine rule 2LV with the monotonic property of $(A_n^{(max)})$ found in Sec. V. The result of such a combination is illustrated in Fig. 8, in the plane $A_n^{(max)} \times \theta_n^{(min,max)}$. Colors indicate the predicted regime durations Δt_{n+1} . A first observation is that regions with larger values of Δt_{n+1} are associated with large (small) values of $A_n^{(max)}$ and $\theta_n^{(max)}$ ($\theta_n^{(min)}$). The inset of Fig. 8(a) is a magnification of one of such regions. Here, the remarkable property is that, even though the color palette is smooth, colors related to Δt_{n+1} become discrete and clearly separated in this plane. This is even more pronounced for larger values of Δt_{n+1} and is better visible

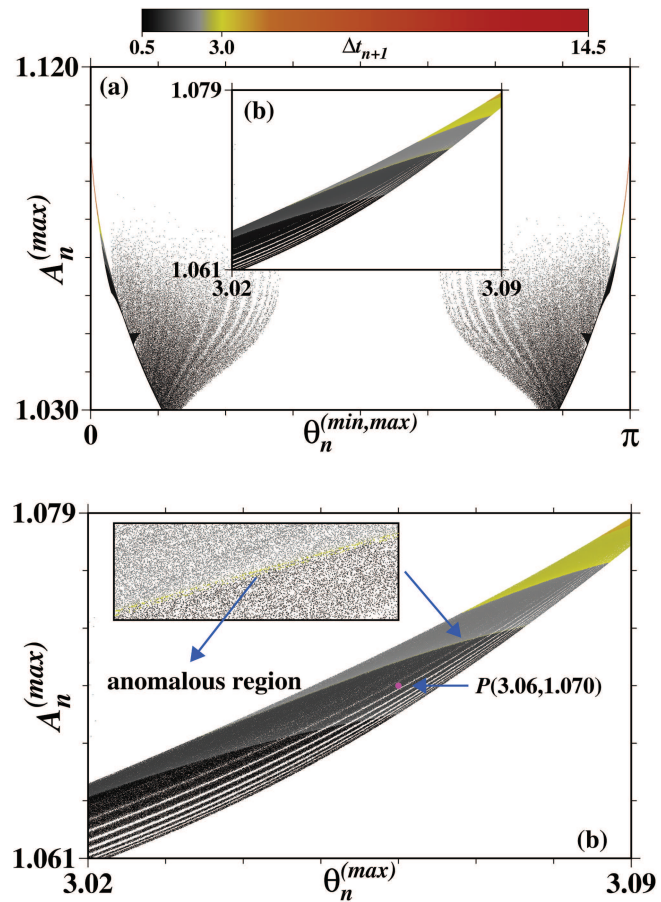


FIG. 8. Plane $A_n^{(max)} \times \theta_n^{(min,max)}$ and colors indicating the predicted regime duration (Δt_{n+1}). The inset in (a) is a magnification of a region close to $\theta_n^{(max)} = \pi$. (b) Magnification of the inset of (a) showing one example of an anomalous region.

in the magnification shown in Fig. 8(b). In other words, for specific values of $A_n^{(max)}$ and $\theta_n^{(min,max)}$, cluster superposition is drastically diminished, thereby allowing a much better estimation of the associated Δt_{n+1} . One example of such an improvement can be given for the point $P = (3.06, 1.070)$, for which we can determine the duration of the regime within the values of the region in medium gray; thus, $\Delta t_{n+1} \approx 1.5$. The same is not possible if we individually take the values of $A_n^{(max)}$ or $\theta_n^{(min,max)}$, as shown in the insets of Figs. 4 and 7.

We apply the k -NN method as a predictor to quantify the improvement in the forecast as a result of considering the two information, $\theta_n^{(min,max)}$ and $A_n^{(max)}$, compared to the forecast obtained with only one information, as shown in Sec. IV. For this, we randomly separated the dataset into two subsets of the same size, one with the test points and the other with the references. We consider the same range of angles as in Sec. IV, which is $3.02 \leq \theta_n^{(max)} \leq 3.09$, but now with all associated $A_n^{(max)}$ values. With the proposed technique, we obtained $MSE \approx 0.006$, which is two orders of magnitude

less than the result from the step function and 33 times less than the result obtained with k -NN considering just one quantity as information.

There are still some anomalous regions, as exemplified in the magnification shown in Fig. 8(b). It shows that for a given pair in the plane $A_n^{(\max)} \times \theta_n^{(\min, \max)}$, which is inside the anomalous region, the predicted time $\Delta t_{n+1} \approx 3.0$ (yellow color) is very close to points in the plane related to the yellow colors in the upper right corner of Fig. 8(b). However, anomalous regions are relatively small when compared to the whole plane $A_n^{(\max)} \times \theta_n^{(\min, \max)}$.

VII. CONCLUSIONS

In this work, we used the alignment of Lyapunov vectors to predict regime changes and regime durations for the standard Lorenz model of atmospheric convection. For the parameters chosen here, the Lyapunov spectrum obeys $\lambda_1 > 0$, $\lambda_2 = 0$, and $\lambda_3 < 0$, which are associated, respectively, with the unstable manifold direction, the flow direction, and the stable manifold direction. We show that each time the angle between the unstable direction and the flow direction satisfies the *alignment conditions*, namely, $\theta \rightarrow 0$ or $\theta \rightarrow \pi$, a regime change occurs *after* the alignment. Our results give a nice mathematical demonstration of the adequacy of combining bred vectors³⁰ with the LV alignment to predict regime durations.

A very promising tool extracted here from the alignment of LVs is applied to predict the regime duration Δt_{n+1} . This quantity provides a monotonic relation between the alignment of vectors $\theta_n^{(\min, \max)}$ and Δt_{n+1} . Such a relation was well described by the adjusted curves given by Eqs. (4) and (5). In addition, we have also shown that a monotonic relation exists between the maxima of the increasing rate ($A_n^{(\max)}$) of the bred vectors and Δt_{n+1} . The adjusted curve for this relation is given by Eq. (8). As shown, certain errors in the predictions may occur due to the clustering of points around specific values of Δt_{n+1} . Such a drawback occurs both for LVs and $A_n^{(\max)}$. Fortunately, such errors can be significantly decreased by combining results obtained from Lyapunov vectors with those from bred vectors. In other words, combining the alignment of LVs and $A_n^{(\max)}$ in just one plane, Δt_{n+1} values tend to become discrete and separated in such a plane. This allows us to predict regime duration with a much better accuracy. We apply the k -NN method as a predictor to quantify the improvement in the forecast as a result of considering the two information, $\theta_n^{(\min, \max)}$ and $A_n^{(\max)}$, compared to the forecast obtained with only one information. With the proposed technique, we obtained 33 times less error than the result obtained with k -NN considering just one quantity as information.

ACKNOWLEDGMENTS

This work was done in the framework of the Advanced Study Group *Forecasting with Lyapunov vectors* at the Max Planck Institute for the Physics of Complex Systems, Dresden, Germany. The authors were supported by CNPq (Grant Nos. 304719/2015-3 and 310792/2018-5), Brazil.

DATA AVAILABILITY

The data that support the findings of this study are available within the article.

REFERENCES

- ¹V. Lucarini, D. Faranda, J. M. Milhazes de Freitas, M. Holland, T. Kuna, M. Nicol, M. Todd, S. Vaienti *et al.*, *Extremes and Recurrence in Dynamical Systems* (John Wiley & Sons, 2016).
- ²E. L. Brugnago, T. A. Hild, D. Weingärtner, and M. W. Beims, "Classification strategies in machine learning techniques predicting regime changes and durations in the Lorenz system," *Chaos* **30**, 053101 (2020).
- ³M. W. Beims and J. A. C. Gallas, "Alignment of Lyapunov vectors: A quantitative criterion to predict catastrophes?," *Sci. Rep.* **6**, 37102 (2016).
- ⁴M. W. Beims and J. A. C. Gallas, "Predictability of the onset of spiking and bursting in complex chemical reactions," *Phys. Chem. Chem. Phys.* **20**, 18539–18546 (2018).
- ⁵E. N. Lorenz, "Deterministic nonperiodic flow," *J. Atmos. Sci.* **20**, 130–141 (1963).
- ⁶F. Ginelli, P. Poggi, A. Turchi, H. Chaté, R. Livi, and A. Politi, "Characterizing dynamics with covariant Lyapunov vectors," *Phys. Rev. Lett.* **99**, 130601 (2007).
- ⁷Y. C. Lai, C. Grebogi, J. A. Yorke, and I. Kan, "How often are chaotic saddles nonhyperbolic?," *Nonlinearity* **6**, 779–797 (1993).
- ⁸C. L. Wolfe and R. M. Samelson, "An efficient method for recovering Lyapunov vectors from singular vectors," *Tellus A* **59**, 355–366 (2007).
- ⁹A. Norwood, E. Kalnay, K. Ide, S. C. Yang, and C. Wolfe, "Lyapunov, singular and bred vectors in a multi-scale system: An empirical exploration of vectors related to instabilities," *J. Phys. A* **46**, 254021 (2013).
- ¹⁰P. V. Kuptsov and U. Parlitz, "Theory and computation of covariant Lyapunov vectors," *J. Nonlinear Sci.* **22**, 727–762 (2012).
- ¹¹F. Ginelli, H. Chaté, R. Livi, and A. Politi, "Covariant Lyapunov vectors," *J. Phys. A* **46**, 254005 (2013).
- ¹²D. P. Truant and G. P. Morriss, "Backward and covariant Lyapunov vectors and exponents for hard-disk systems with a steady heat current," *Phys. Rev. E* **90**, 052907 (2014).
- ¹³P. V. Kuptsov and A. V. Kuptsova, "Predictable nonwandering localization of covariant Lyapunov vectors and cluster synchronization in scale-free networks of chaotic maps," *Phys. Rev. E* **90**, 032901 (2014).
- ¹⁴M. Inubushi, S. Takehiro, and M. Yamada, "Regeneration cycle and the covariant Lyapunov vectors in a minimal wall turbulence," *Phys. Rev. E* **92**, 023022 (2015).
- ¹⁵L. Palatella, A. Trevisan, and S. Rambaldi, "Nonlinear stability of traffic models and the use of Lyapunov vectors for estimating the traffic state," *Phys. Rev. E* **88**, 022901 (2013).
- ¹⁶T. S. Krüger, P. P. Galuzio, T. L. Prado, R. L. Viana, J. D. Szezech, and S. R. Lopes, "Mechanism for stickiness suppression during extreme events in Hamiltonian systems," *Phys. Rev. E* **91**, 062903 (2015).
- ¹⁷C. A. Jousseph, T. S. Krüger, C. Manchein, S. R. Lopes, and M. W. Beims, "Weak dissipative effects on trajectories from the edge of basins of attraction," *Physica A* **456**, 68–74 (2016).
- ¹⁸R. S. Hansen and S. Hannestad, "Chaotic flavor evolution in an interacting neutrino gas," *Phys. Rev. D* **90**, 025009 (2014).
- ¹⁹Y. Pomeau, A. Pumir, and P. Pelce, "Intrinsic stochasticity with many degrees of freedom," *J. Stat. Phys.* **37**, 39–49 (1984).
- ²⁰M. W. Beims and J. A. C. Gallas, "Manifold angles, the concept of self-similarity, and angle-enhanced bifurcation diagrams," *Sci. Rep.* **6**, 18859 (2016).
- ²¹M. Sala, C. Manchein, and R. Artuso, "Estimating hyperbolicity of chaotic bidimensional maps," *Int. J. Bifurcat. Chaos* **22**, 1250217 (2012).
- ²²A. Trevisan and F. Pancotti, "Periodic orbits, Lyapunov vectors, and singular vectors in the Lorenz system," *J. Atmos. Sci.* **55**, 390–398 (1998).
- ²³Y. Saiki and M. U. Kobayashi, "Numerical identification of nonhyperbolicity of the Lorenz system through Lyapunov vectors," *JSIAM Lett.* **2**, 107–110 (2010).

²⁴N. Sharafi, M. Timme, and S. Hallerberg, “Critical transitions and perturbation growth directions,” *Phys. Rev. E* **96**, 032220 (2017).

²⁵C. Sparrow, *The Lorenz Equations: Bifurcations, Chaos, and Strange Attractors* (Springer Science & Business Media, 2012), Vol. 41.

²⁶E. Evans, N. Bhatti, J. Kinney, L. Pann, M. Peña, S. C. Yang, E. Kalnay, and J. Hansen, “Rise undergraduates find that regime changes in Lorenz’s model are predictable,” *Bull. Am. Meteorol. Soc.* **85**, 520–524 (2004).

²⁷R. S. Yadav, S. Dwivedi, and A. K. Mittal, “Prediction rules for regime changes and length in a new regime for the Lorenz model,” *J. Atmos. Sci.* **62**, 2316–2321 (2005).

²⁸Y. Song, J. Liang, J. Lu, and X. Zhao, “An efficient instance selection algorithm for k nearest neighbor regression,” *Neurocomputing* **251**, 26–34 (2017).

²⁹Y. Mack, “Local properties of k-NN regression estimates,” *SIAM J. Alg. Discret. Meth.* **2**, 311–323 (1981).

³⁰Y. Zhang, K. Ide, and E. Kalnay, “Bred vectors of the Lorenz63 system,” *Adv. Atmos. Sci.* **32**, 1533–1538 (2015).

³¹E. L. Brugnago, J. A. C. Gallas, and M. W. Beims, “Machine learning, alignment of covariant Lyapunov vectors and predictability in Rikitake’s geomagnetic dynamo model,” *Chaos* **30**, 083106 (2020).